Physical Processes Leading to Extreme day-to-day Temperatures Changes, Part I: Present-day Climate

Kalpana Hamal and Stephan Pfahl

Institut für Meteorologie, Freie Universität Berlin, 12165 Berlin., Germany

Correspondence to: Kalpana Hamal (*k.hamal@fu-berlin.de*)

Supplementary File

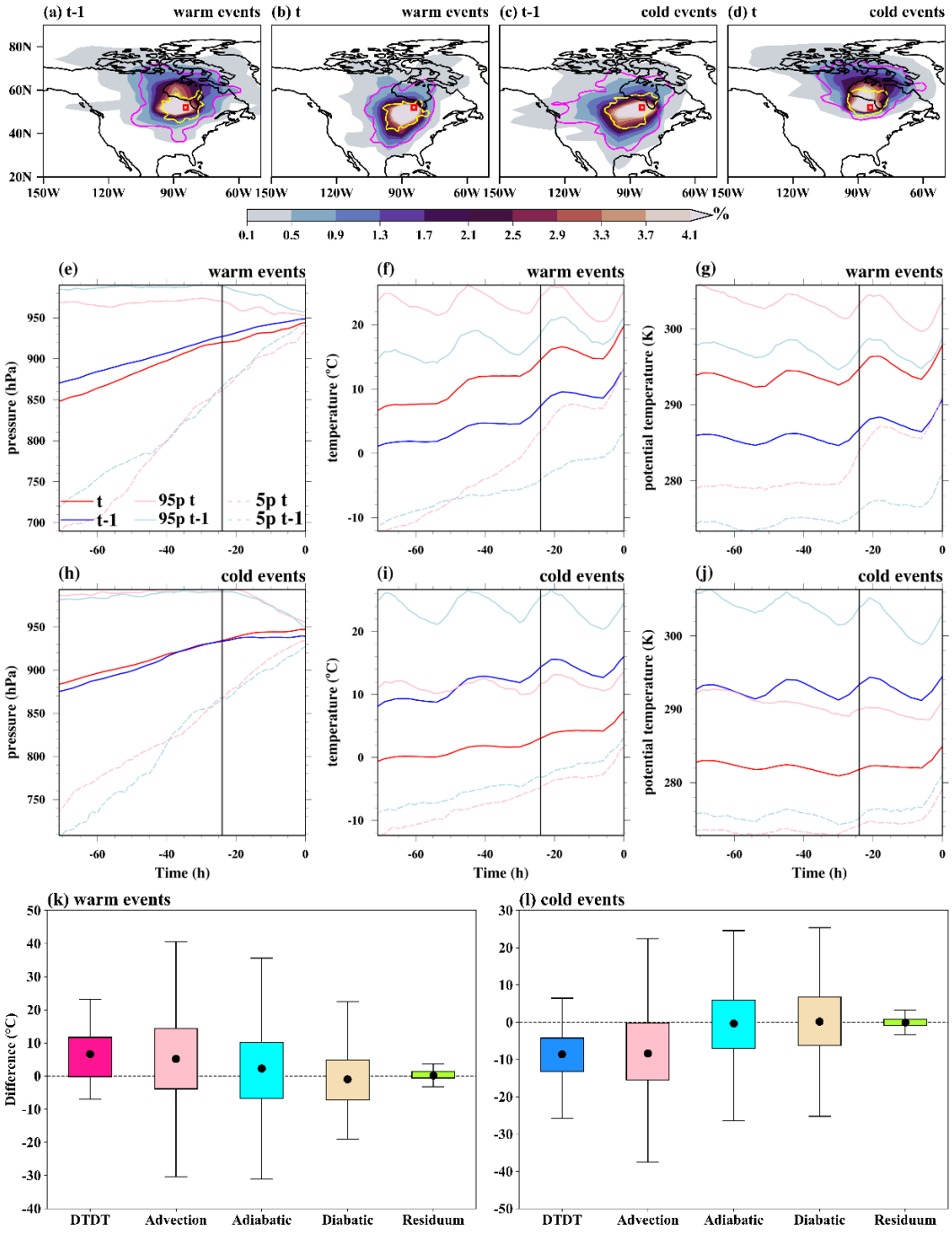

Figure S1. The spatial distribution of trajectories initiated on the previous day (t-1) and event day (t) for both June-August (JJA) warm and cold events over North America. In the top row, the color-shading illustrates the air parcel trajectory density (%) based on the position between -5d and 0d. The magenta and yellow contours represent 0.5% particle density fields at -3d and -1d, respectively. The red box shows the selected grid point over North America. The Lagrangian evolution of distinct physical parameters (pressure, temperature, potential temperature) along the air parcel trajectories for both warm (2nd row) and cold

events (3rd row) is presented in panels e-j. Panels k and l show the contribution of the different physical processes to the genesis of DTDT extremes according to Eq. (6), which refers to a 3d-time scale. The residuum is attributable to numerical inaccuracies in the computation of derivatives in Eq. (6). The box spans the 25th and 75th percentile of the data; the black dot inside the box gives the mean of the related quantities, and 1.5 times the interquartile range is indicated by the whiskers.

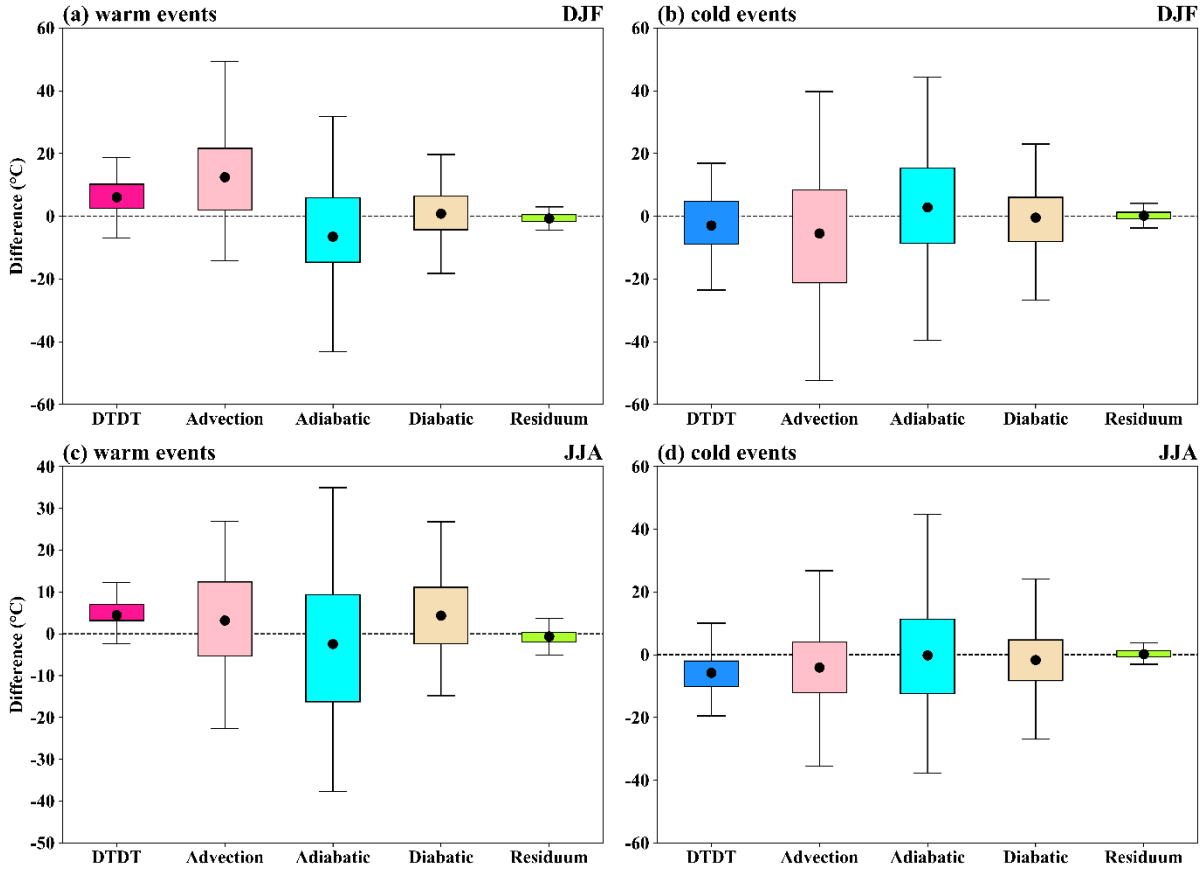

Figure S2. The contribution of the different physical processes (advection, adiabatic, and diabatic) to the genesis of DTDT extremes over western North America (120°W and 45°N) according to Eq. (6), which refers to a 3d-time scale during (a, b) December-February (DJF) and (c,d) June-August (JJA). The residuum is attributable to numerical inaccuracies in the computation of derivatives in Eq. (6). The box spans the 25th and 75th percentile of the data; the black circle inside the box gives the mean of the related quantities, and 1.5 times the interquartile range gives the whiskers.

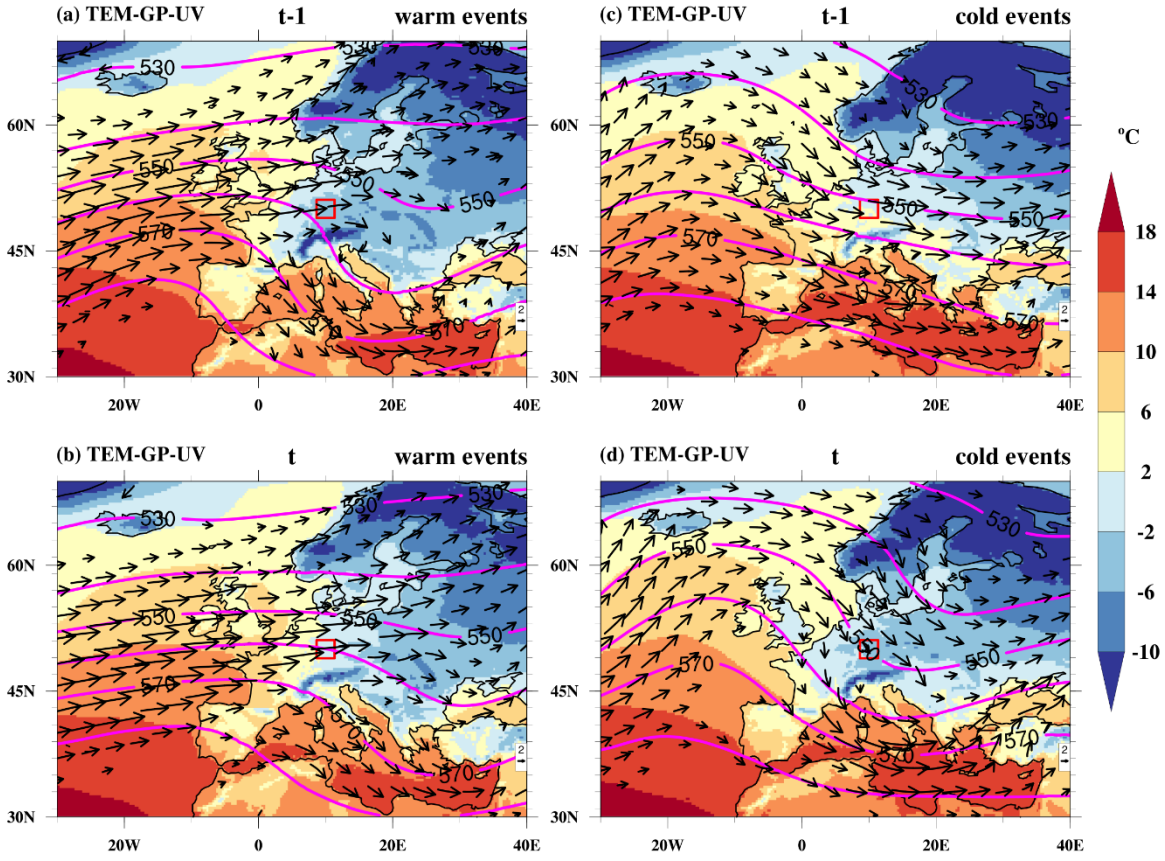

Figure S3. Composite of near-surface temperature (TEM, °C, color shading), wind at 850 hPa (UV, m/s, vectors), and Geopotential height at 500 hPa (GP, gpm, magenta contours) on the (a, c) previous day (t-1) and (b, d) event day (t) of the warm (a,b) and cold events (c,d) during December-February (DJF) at a selected grid point in Europe (red box). Note that wind vectors ≥5m/s are plotted.

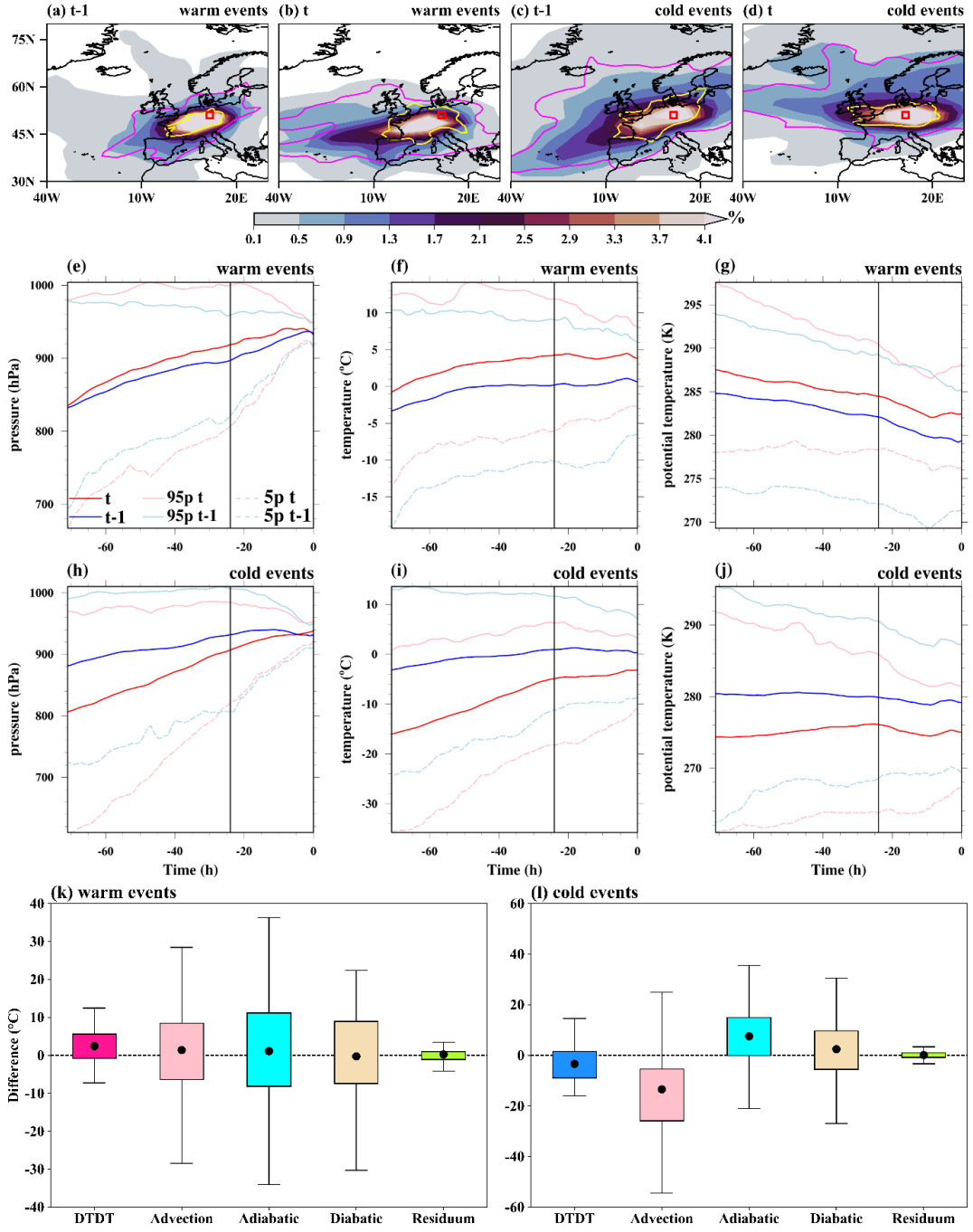

Figure S4. The spatial distribution of trajectories initiated on the previous day (t-1) and the event day (t) for both December (DJF) warm and cold events over Europe. In the top row, the color-shading illustrates the air parcel trajectory density (%) based on the position between -5d and 0d. The magenta and yellow contours represent 0.5% particle density fields at -3d and -1d, respectively. The red box shows the selected grid point over Europe. The Lagrangian evolution of distinct physical parameters (pressure, temperature, potential temperature) along the air parcel trajectories for both warm (2nd row) and cold events (3rd row) is

presented in panels e-j. Panels k and l show the contribution of the different physical processes to the genesis of DTDT extremes according to Eq. (6), which refers to a 3d-time scale. The residuum is attributable to numerical inaccuracies in the computation of derivatives in Eq. (6). The box spans the 25th and 75th percentile of the data; the black circle inside the box gives the mean of the related quantities, and 1.5 times the interquartile range gives the whiskers.

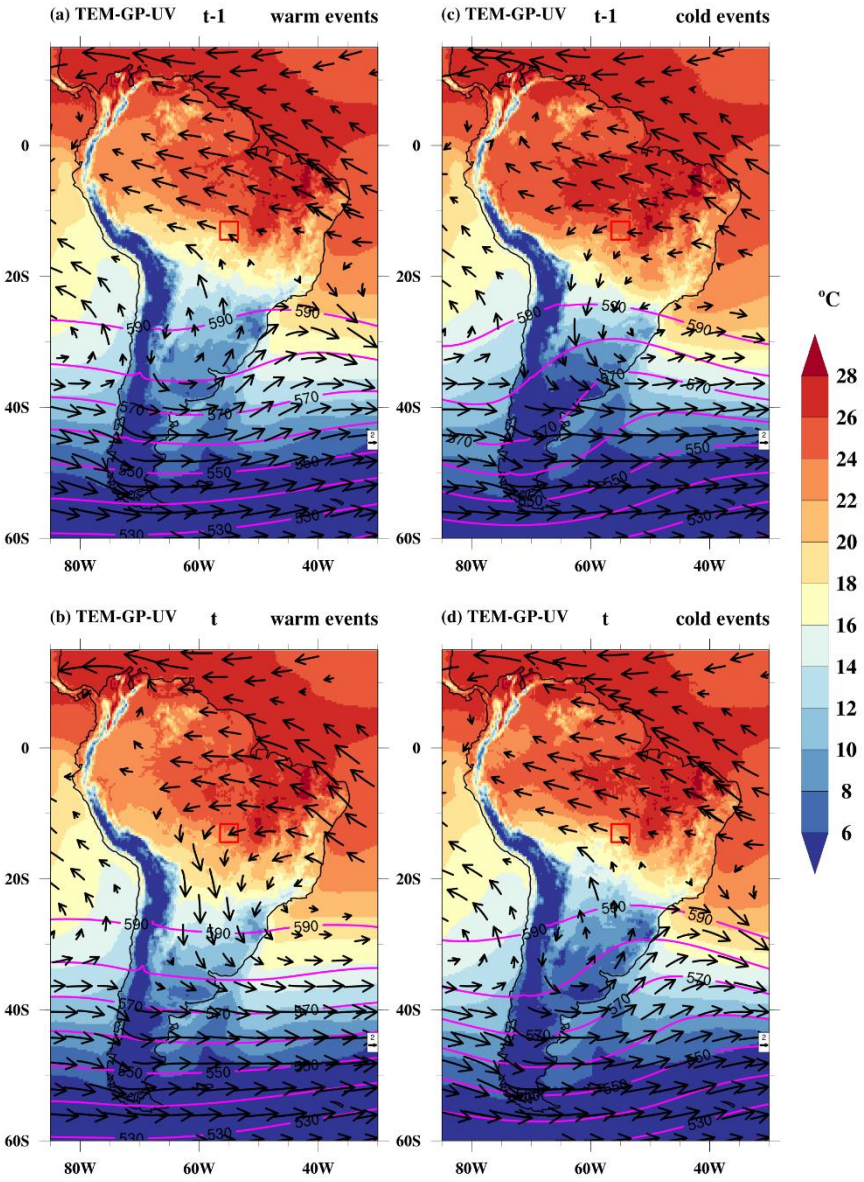

Figure S5. Composite of near-surface temperature (TEM, °C, color shading), wind at 850 hPa (UV, m/s, vectors), and Geopotential height at 500 hPa (GP, gpm, magenta contours) on the (a, c) previous day (t-1) and (b, d) event day (t) of the warm events (a,b) and cold events (c,d) during June-August (JJA) at a selected grid point in South America (red box). Note that wind vectors ≥2.5m/s are plotted.

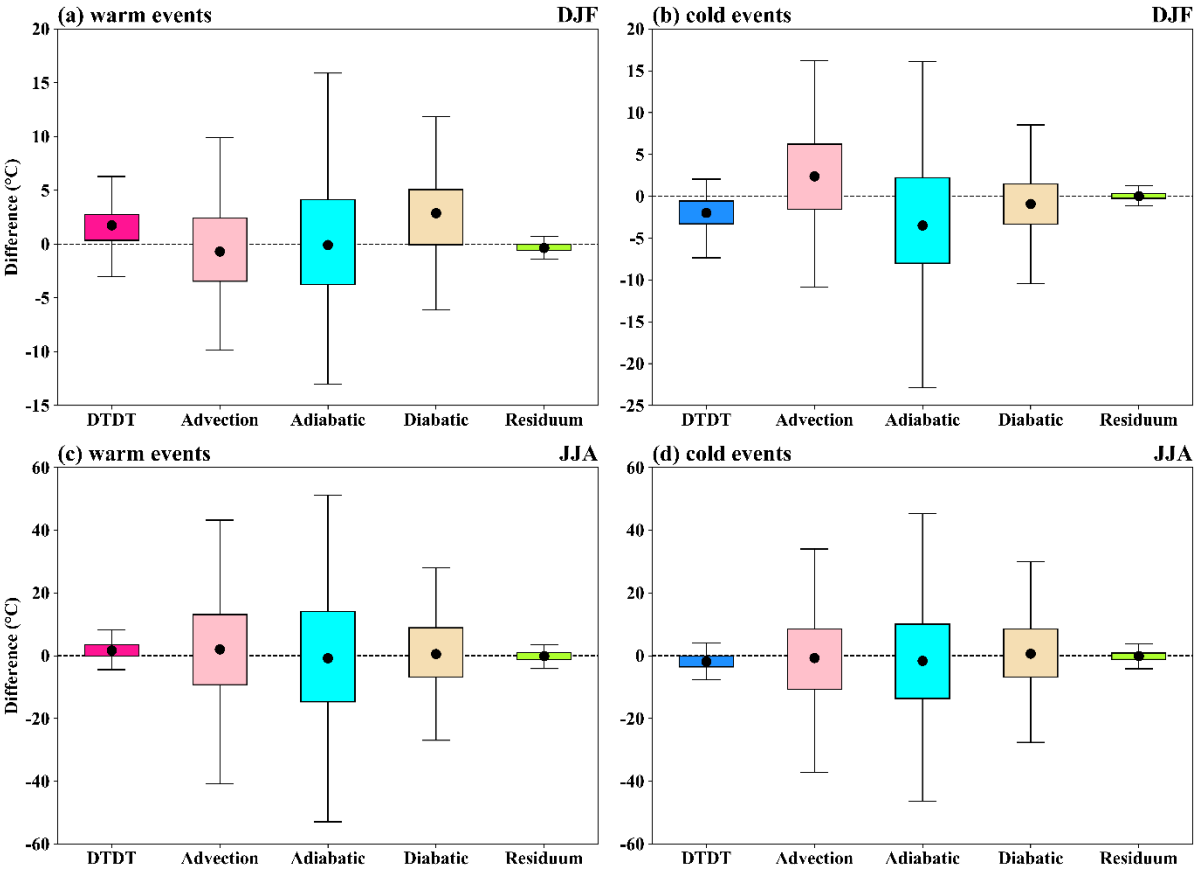

Figure S6. The contribution of the different physical processes (advection, adiabatic, and diabatic) to the genesis of DTDT extremes over South Africa (24°E and 13°S) according to Eq. (6), which refers to a 3d-time scale during (a, b) December-February (DJF) and (c,d) June-August (JJA). The residuum is attributable to numerical inaccuracies in the computation of derivatives in Eq. (6). The box spans the 25th and 75th percentile of the data; the black circle inside the box gives the mean of the related quantities, and 1.5 times the interquartile range gives the whiskers.

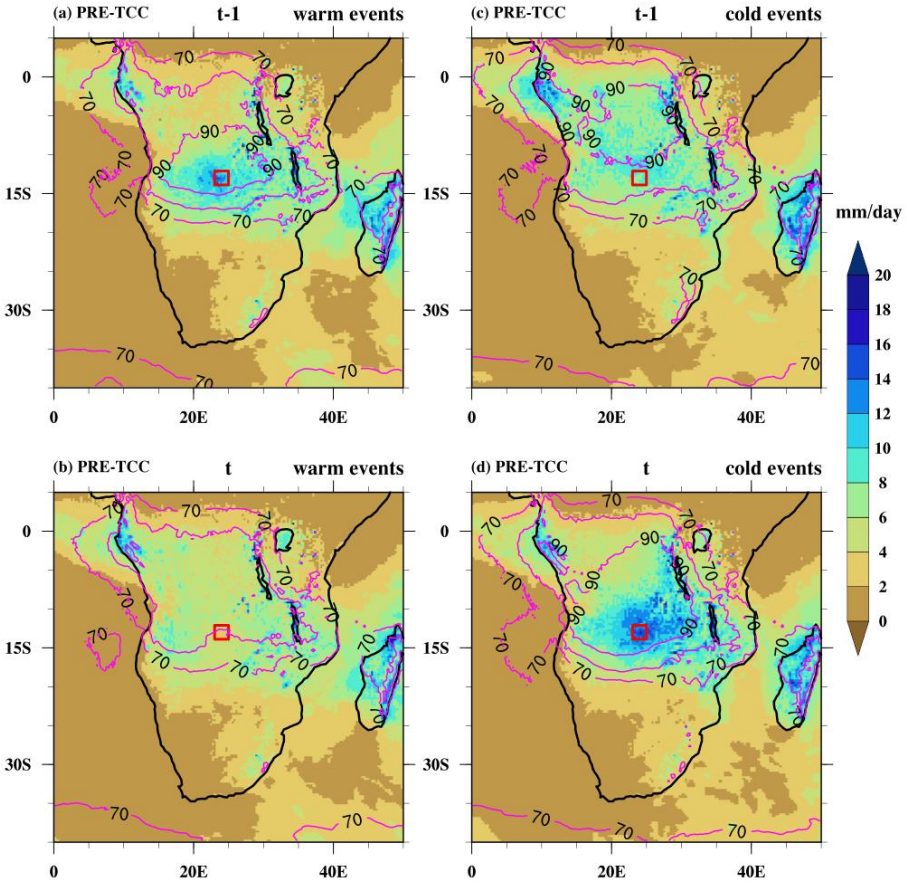

Figure S7. Composites of precipitation (PRE, mm/day, color shading) and Total cloud cover (TCC, %, magenta contours) on the (a, c) previous day (t-1) and (b, d) event day (t) of warm (a,b) and cold events (c,d) during December-February (DJF) at a selected grid point in South Africa (24°E and 13°S, red box).

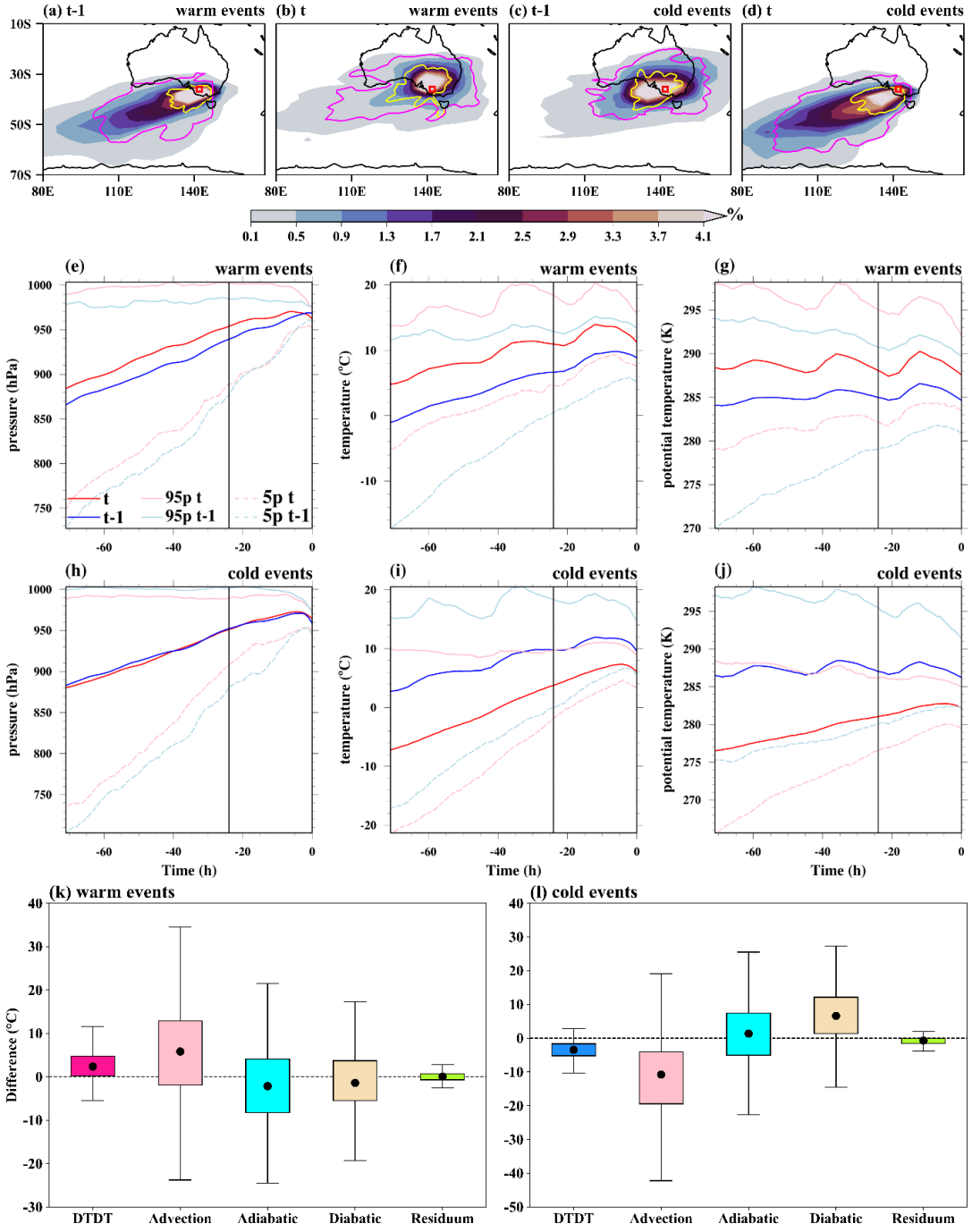

Figure S8. The spatial distribution of trajectories initiated on the previous day (t-1) event day (t) for both June-August (JJA) warm and cold events over Australia. In the top row, the color-shading illustrates the air parcel trajectory density (%) based on the position between -5d and 0d. The magenta and yellow contours represent 0.5% particle density fields at -3d and -1d, respectively. The red box shows the selected grid point over Australia. The Lagrangian evolution of distinct physical parameters (pressure, temperature, potential temperature) along the air parcel trajectories for both warm (2nd row) and cold events (3rd

row) is presented in panels e-j. Panels k and l show the contribution of the different physical processes to the genesis of DTDT extremes according to Eq. (6), which refers to a 3d-time scale. The residuum is attributable to numerical inaccuracies in the computation of derivatives in Eq. (6). The box spans the 25th and 75th percentile of the data; the black circle inside the box gives the mean of the related quantities, and 1.5 times the interquartile range gives the whiskers.

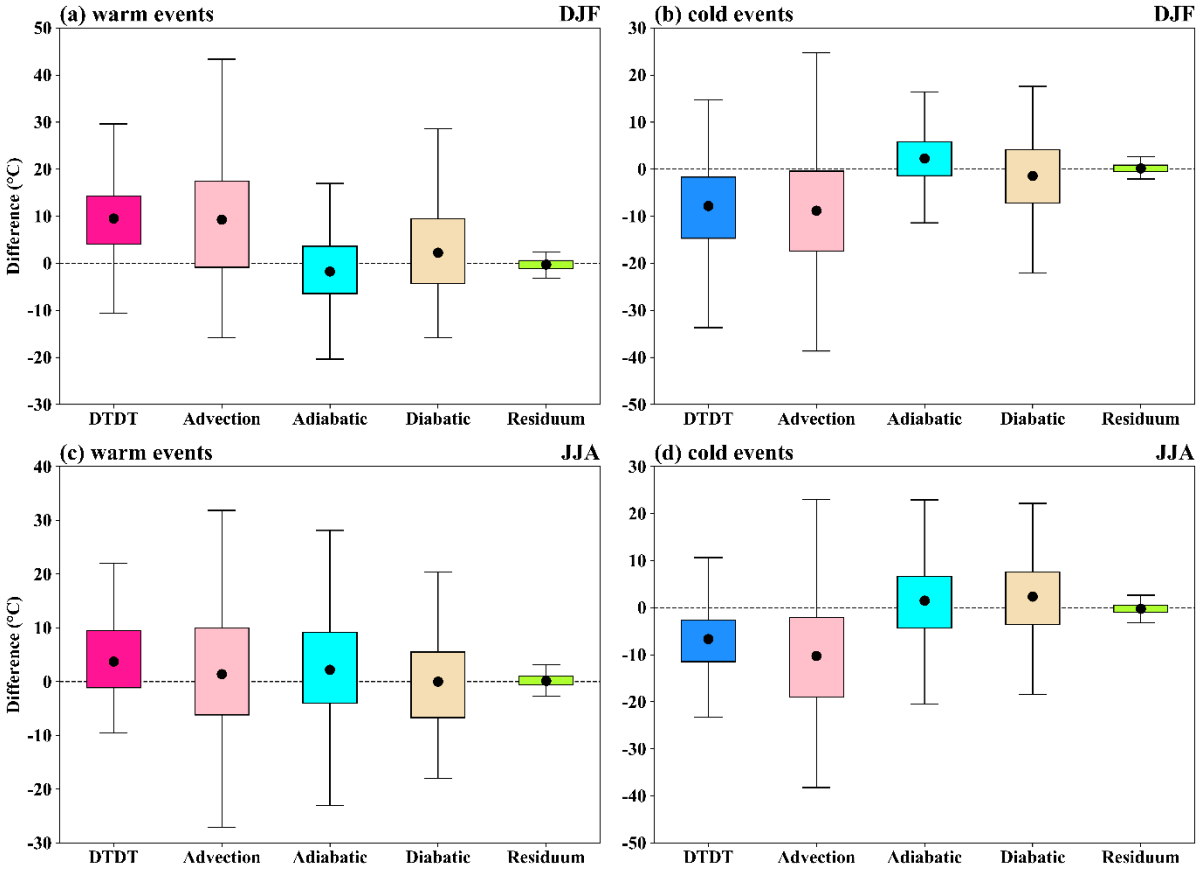

Figure S9. The contribution of the different physical processes (advection, adiabatic, and diabatic) to the genesis of DTDT extremes over high latitude-North Asia (90°E and 70°N) according to Eq. (6), which refers to a 3d-time scale during (a, b) December-February (DJF) and (c,d) June-August (JJA). The residuum is attributable to numerical inaccuracies in the computation of derivatives in Eq. (6). The box spans the 25th and 75th percentile of the data; the black circle inside the box gives the mean of the related quantities, and 1.5 times the interquartile range gives the whiskers.

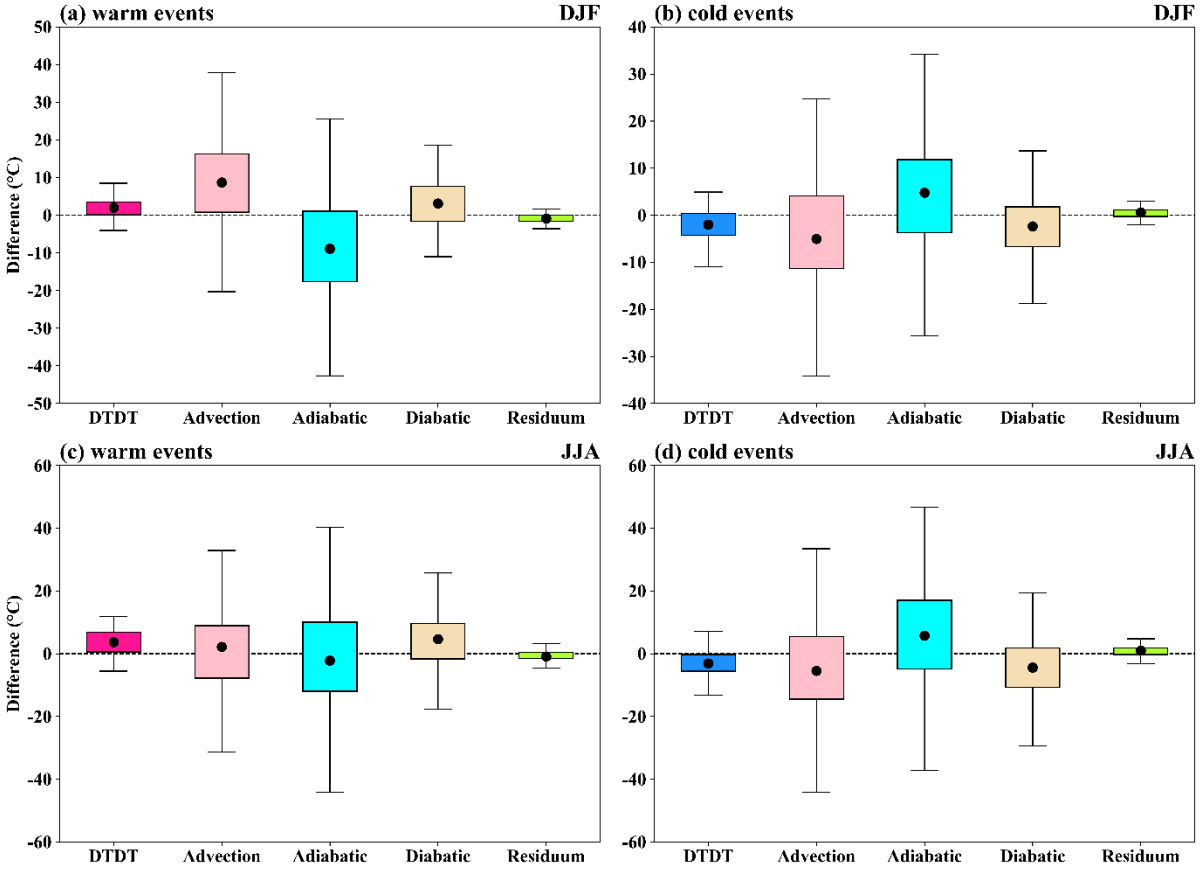

Figure S10. The contribution of the different physical processes (advection, adiabatic, and diabatic) to the genesis of DTDT extremes over subtropics-South Asia (80°E and 23°N) according to Eq. (6), which refers to a 3d-time scale during (a, b) December-February (DJF) and (c,d) June-August (JJA). The residuum is attributable to numerical inaccuracies in the computation of derivatives in Eq. (6). The box spans the 25th and 75th percentile of the data; the black circle inside the box gives the mean of the related quantities, and 1.5 times the interquartile range gives the whiskers.